High-Latitude Atmospheric Motion Vectors from Composite Satellite Data

MATTHEW A. LAZZARA

Antarctic Meteorological Research Center, and Cooperative Institute for Meteorological Satellite Studies, Space Science and Engineering Center, University of Wisconsin—Madison, Madison, Wisconsin

RICHARD DWORAK, DAVID A. SANTEK, BRETT T. HOOVER, AND CHRISTOPHER S. VELDEN

Cooperative Institute for Meteorological Satellite Studies, Space Science and Engineering Center, University of Wisconsin—Madison, Madison, Wisconsin

JEFFREY R. KEY

NOAA/NESDIS/Center for Satellite Applications and Research, Madison, Wisconsin

(Manuscript received 11 May 2013, in final form 19 September 2013)

ABSTRACT

Atmospheric motion vectors (AMVs) are derived from satellite-observed motions of clouds and water vapor features. They provide crucial information in regions void of conventional observations and contribute to forecaster diagnostics of meteorological conditions, as well as numerical weather prediction. AMVs derived from geostationary (GEO) satellite observations over the middle latitudes and tropics have been utilized operationally since the 1980s; AMVs over the polar regions derived from low-earth (polar)-orbiting (LEO) satellites have been utilized since the early 2000s. There still exists a gap in AMV coverage between these two sources in the latitude band poleward of 60° and equatorward of 70° (both hemispheres). To address this AMV gap, the use of a novel approach to create image sequences that consist of composites derived from a combination of LEO and GEO observations that extend into the deep middle latitudes is explored. Experiments are performed to determine whether the satellite composite images can be employed to generate AMVs over the gap regions. The derived AMVs are validated over both the Southern Ocean/Antarctic and the Arctic gap regions over a multiyear period using rawinsonde wind observations. In addition, a two-season numerical model impact study using the Global Forecast System indicates that the assimilation of these AMVs can improve upon the control (operational) forecasts, particularly during lower-skill (dropout) events.

1. Introduction

For decades, atmospheric motion vectors (AMVs) have been derived using geostationary satellite data (Velden et al. 2005) and separately from polar-orbiting satellites (Key et al. 2003). However, at higher latitudes in both hemispheres there is a gap in coverage between these two observational datasets in the latitudinal zone from approximately 60° to 70° (Fig. 1). This has inspired an investigation into using composite satellite imagery—a combination of geostationary (GEO) and polar [low-earth-orbit (LEO)] images (Lazzara et al. 2003, 2011)—to generate AMVs in this gap (henceforth referred to as LEO–GEO AMVs).

The polar branch of the jet stream can often be found at these latitudes (Palmén and Newton 1969), and accurate analysis of the strength and position of the polar jet is critical for skillful numerical weather prediction (NWP) in the middle latitudes (Santek 2010). With significant commercial aircraft routing over the Arctic and increasing flights to the Antarctic continent, the lack of in situ or satellite wind observations in this region can have important aviation implications.

Utilizing sequences of composites created from a mosaic of LEO and GEO observations that have coverage from the pole into the middle latitudes makes it

Denotes Open Access content.

Corresponding author address: Matthew A. Lazzara, Antarctic Meteorological Research Center, Space Science and Engineering Center, University of Wisconsin—Madison, 1225 West Dayton St., Madison, WI 53706.
E-mail: mattl@ssec.wisc.edu

DOI: 10.1175/JAMC-D-13-0160.1

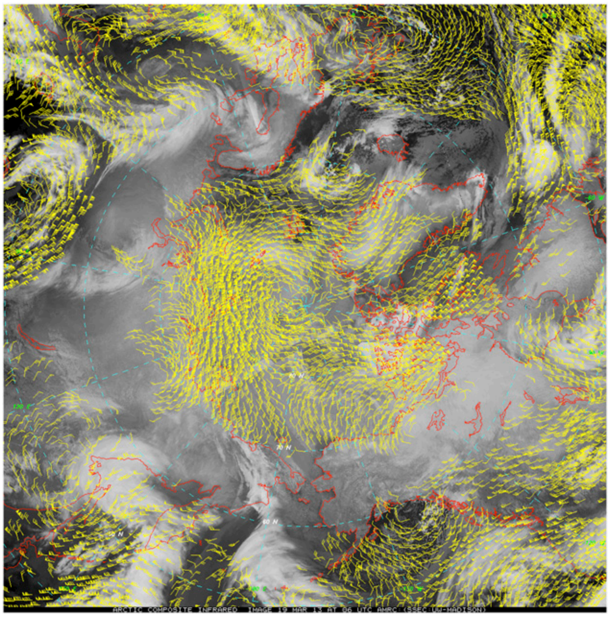

FIG. 1. Example of AMVs from geostationary satellite observations and polar-orbiting satellite observations over the Northern Hemisphere for a 6-h period on 19 Mar 2013. An observational gap in coverage exists between the two processed AMV datasets in the 60°–70° latitude band, shown over a corresponding 0600 UTC Arctic composite satellite image.

possible to investigate the generation of AMVs in this gap region. The resulting LEO–GEO AMVs are validated and then employed in a two-season numerical model impact study to establish if the assimilation of these AMVs can improve upon operational weather forecasts. The data and methodology used to produce the composite imagery and the LEO–GEO AMVs are described in section 2. The validation of the AMVs against available rawinsonde observations is presented in section 3.

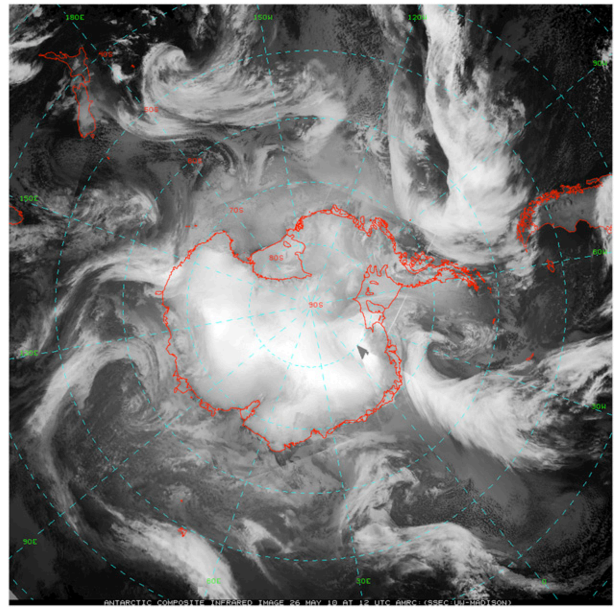

FIG. 2. A sample Antarctic infrared composite image from 1200 UTC 26 May 2010.

Experiments that demonstrate the forecast impact of LEO–GEO AMVs are discussed in section 4. Conclusions on the potential applications of this product are given in section 5.

2. Data and method

The following sections detail the heritage composite generation, the original LEO–GEO wind product, and the improved LEO–GEO wind generation, which depends on a new composite technique and the use of additional pixel-level information (e.g., time and parallax) in the AMV determination.

TABLE 1. Satellites used to make the Arctic and Antarctic composite imagery.

Geostationary		Polar orbiting	
Satellite series	Satellites	Satellite series	Satellites
GOES	*GOES-East* *GOES-West* *GOES-South America*	Polar-Orbiting Operational Environmental Satellite (POES)	*NOAA-15* *NOAA-16* *NOAA-18* *NOAA-19*
Meteosat (at 0° and 57°E)	*Meteosat-7* *Meteosat-8* *Meteosat-9*	Earth Observing System (EOS)	*Terra* *Aqua*
Multi-Functional Transport Satellite (MTSAT)	*MTSAT-1R* *MTSAT-2*	European Organisation for the Exploitation of Meteorological Satellites (EUMETSAT) Polar-Orbiting System (EPS)	*Meteorological Operational-A* (*MetOp-A*) *MetOp-B*
Fen Yung-2	*FY-2C* *FY-2D* *FY-2E*		

a. Arctic and Antarctic satellite composites

Satellite image composites have been generated at the University of Wisconsin Space Science and Engineering Center (UW-SSEC) over the Antarctic for over 20 yr (Lazzara et al. 2003, 2011; Kohrs et al. 2013), and over the Arctic for approximately 5 yr (Lazzara and Knuth 2009; Lazzara et al. 2011; Kohrs et al. 2013). These composites are a mosaic of satellite images from both polar and geostationary platforms. Once individual images are received at UW-SSEC, the data are reprojected onto a standard polar stereographic grid. Close-in-time images are then merged (Fig. 2), with GEO first and LEO last via a conditional minimum method to take into account limb darkening (Minnis 1989; Joyce et al. 2001). In this method, the darkest, nonzero brightness pixel is selected to be used in the final composite image.

A variety of currently operating GEO and LEO satellites are used to produce the composites (Table 1), and new satellites are added as they become available. The composites are produced for several spectral channels, including the infrared window, water vapor, visible, and shortwave infrared. The source satellite observations that go into each composite image are reprojected or remapped into a polar stereographic projection that is defined as having a nominal resolution of 5 km at the standard latitude of 60°. When the composites are created, the highest resolution imagery is always placed on top when combining the imagery. From geostationary satellites at this latitude, the resolution of Geostationary Operational Environmental Satellite (GOES) imagery is roughly 11.5 km × 2.5 km. However, an image from a polar-orbiting satellite is produced at much higher resolution; the resolution of the Advanced Very High Resolution Radiometer (AVHRR) Global Area Coverage data, for example, is 3 km × 5 km. While the geostationary satellite data are of lower resolution than the polar data at these latitudes, the geostationary observations provide time continuity while the polar-orbiting data offer high spatial resolution. The reprojection from the original satellite view to this geographic projection reduces the distortion of the cloud features. Details about these composites can be found in Kohrs et al. (2013). The infrared window channel is the focus of the AMVs generated in this project.

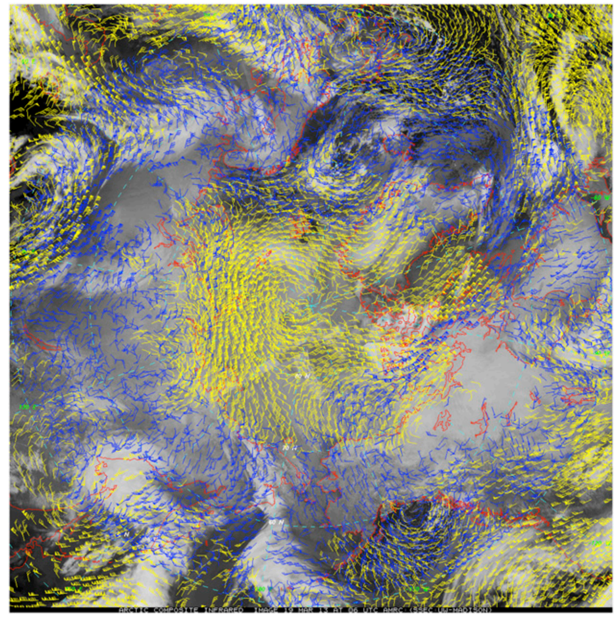

FIG. 3. As in Fig. 1, but with composite LEO–GEO AMVs plotted in blue to show how the gap in coverage is bridged.

One requirement for this investigation was to increase the temporal resolution of the composites to 1 h from the traditional 3-h interval found in the Antarctic and Arctic composites generated before the start of this effort (Lazzara et al. 2003; Kohrs et al. 2013), thereby providing image information closer to the temporal frequency used for GEO AMVs—typically hourly (Lazzara et al. 2010). In these second-generation composites used in this project, the spatial resolution of the composites was increased to 4-km nominal resolution. These changes could also benefit operational forecasters in search of higher-resolution image animations to support their efforts. Spectral differences are not specifically accounted for in the generation of these composites. As the focus of the project discussed here is centered on the infrared

TABLE 2. Validation statistics for the composite LEO–GEO AMVs, partitioned by hemisphere and tropospheric layers (vector height assignments). NRMS is RMSE normalized by the mean rawinsonde wind speed.

	Northern Hemisphere				Southern Hemisphere			
	>700 hPa	700–>400 hPa	≤400 hPa	Total	>700 hPa	700–>400 hPa	≤400 hPa	Total
Vector RMSE ($m\,s^{-1}$)	4.81	5.98	7.06	6.21	6.18	7.12	9.19	7.82
Zonal wind bias ($m\,s^{-1}$)	−0.14	−0.39	−0.68	−0.45	+0.89	+0.42	−0.94	0.00
Meridional wind bias ($m\,s^{-1}$)	−0.05	−0.35	+0.16	−0.12	+0.36	−0.38	−2.55	−1.06
Vector NRMS	0.38	0.37	0.28	0.33	0.50	0.49	0.34	0.42
Mean AMV speed ($m\,s^{-1}$)	12.29	15.24	24.36	17.94	13.35	14.06	27.65	18.64
Sample size	19 988	61 041	43 156	124 185	26	169	101	296

TABLE 3. Validation statistics for the composite LEO–GEO AMVs partitioned by latitude bands. NRMS is RMSE normalized by the mean rawinsonde wind speed.

	Northern Hemisphere			Southern Hemisphere		
	≥70°	60°–<70°	50°–<60°	≥70°	60°–<70°	50°–<60°
Vector RMSE (m s^{-1})	7.38	6.20	6.21	8.28	8.17	6.64
Zonal wind bias (m s^{-1})	+0.02	−0.38	−0.48	+0.06	+0.12	−0.68
Meridional wind bias (m s^{-1})	+0.01	−0.25	−0.09	2.85	−1.55	−2.28
Vector NRMS	0.43	0.34	0.33	0.58	0.43	0.28
Mean AMV speed (m s^{-1})	16.96	17.43	18.08	14.02	18.48	23.96
Sample size	908	26 626	96 651	40	215	41

window channel (approximately 11.0 μm), contributing satellites have fairly similar, although not exactly the same, spectral characteristics.

b. AMV generation

The algorithm used for generation of composite LEO–GEO AMVs is very similar to the methods used for the Moderate Resolution Imaging Spectroradiometer (MODIS), the National Oceanic and Atmospheric Administration (NOAA) AVHRR, and GOES AMVs (Nieman et al. 1997; Key et al. 2003). Three time-successive composite images are used to track coherent features. Short-term National Centers for Environmental Prediction (NCEP) Global Forecast System (GFS) model forecasts are used as an aid to assign vector heights.

The first step in the process is to determine potential targets to be tracked. This is done by calculating local bidirectional gradients of brightness temperature in predetermined search box areas in the middle image of the triplet. If an empirically derived gradient threshold is reached, then the estimated pressure height of the target is calculated (Nieman et al. 1997). The height assignment of the target follows the same methodology as outlined in Nieman et al. (1997) via use of the infrared window channel method. This method uses the average of the coldest pixels to determine the height from a vertical profile of temperature. This study did not investigate alternative methods for the height assignment of the selected targets.

Next, for each target, neighboring images (in time, which varies with satellite platform) are searched within a prescribed area box for high feature correlations with the initial target. If successful, two subvectors are then calculated and are compared to one another for coherency and also to the background field to determine initial quality. Any subvectors with unacceptable accelerations or large deviations from the first guess are thrown out. Remaining subvector pairs are then averaged to create AMVs.

A final postprocessing step is to compute a quality indicator (QI) for each AMV (Holmlund et al. 2001). In general, the higher the QI value (maximum value of 1.0), the lower the expected observational error. The primary purpose of assigning a QI to each AMV is to give end users a confidence estimate in the quality of the observation, and also as a potential aid for determining observational weights in data assimilation.

c. Modifications to composite image and AMV generation

For composite LEO–GEO AMV generation, the targeting and tracking of cloud features are constrained to be poleward of 50° latitude in both hemispheres. This overlaps both the LEO and GEO AMV domains. After the production of the LEO–GEO AMVs, the void (Fig. 1) is filled and complete coverage is achieved (Fig. 3).

Although AMVs can be determined from the composite images, the mix of different satellites can result in

TABLE 4. Validation statistics for the composite GEO AMVs only, partitioned by latitude bands. NRMS is RMSE normalized by the mean rawinsonde wind speed.

	Northern Hemisphere			Southern Hemisphere		
	≥70°	60°–<70°	50°–<60°	≥70°	60°–<70°	50°–<60°
Vector RMSE (m s^{-1})	8.74	6.16	5.87	6.80	7.36	7.99
Zonal wind bias (m s^{-1})	−0.61	−0.51	−0.44	+0.77	−0.10	−2.54
Meridional wind bias (m s^{-1})	−0.70	−0.33	−0.20	+1.17	+0.41	−1.16
Vector NRMS	0.50	0.36	0.33	0.57	0.49	0.39
Mean AMV speed (m s^{-1})	15.80	16.33	17.34	10.92	14.15	17.91
Sample size	3780	65 749	300 086	700	1298	429

TABLE 5. Validation statistics for the composite LEO AMVs only, partitioned by latitude bands. NRMS is RMSE normalized by the mean rawinsonde wind speed.

	Northern Hemisphere			Southern Hemisphere		
	≥70°	60°–<70°	50°–<60°	≥70°	60°–<70°	50°–<60°
Vector RMSE (m s^{-1})	5.88	5.74	5.46	5.34	6.86	0
Zonal wind bias (m s^{-1})	−0.16	−0.42	+0.01	+1.35	−0.74	0
Meridional wind bias (m s^{-1})	+0.10	−0.29	−0.15	−0.87	−1.22	0
Vector NRMS	0.45	0.37	0.31	0.50	0.56	0
Mean AMV speed (m s^{-1})	13.17	14.69	17.61	8.97	12.20	0
Sample size	2534	3212	1548	69	100	0

varying times at individual pixels and parallax effects from different viewing geometries. This can have an impact on the quality of the AMVs. To account for these variations in time and geometry, the compositing technique was enhanced to include the following pixel-level metadata: brightness temperature, scan time, pixel distance from the satellite subpoint, pixel area, satellite identification, sensor wavelength, parallax distance, and parallax direction. The AMV algorithm makes use of the metadata to compute the AMV in these composited images. The metadata ensure that the targeted and tracked features contain data only from a single satellite, although the correlating feature in each image of the triplet may be from a different satellite. All the pixels in the target and search boxes have one time associated with them, as the data come from an individual satellite. For example, the middle composite may have a section of a GOES image, and images before and after may have sections from MODIS, for the same feature. Thus the time of the pixels for each feature will be homogeneous. These times are used for computing the AMV and not the nominal image time. Metadata also account for the parallax of the feature being tracked when computing the AMV. Parallax is not corrected when reprojecting the

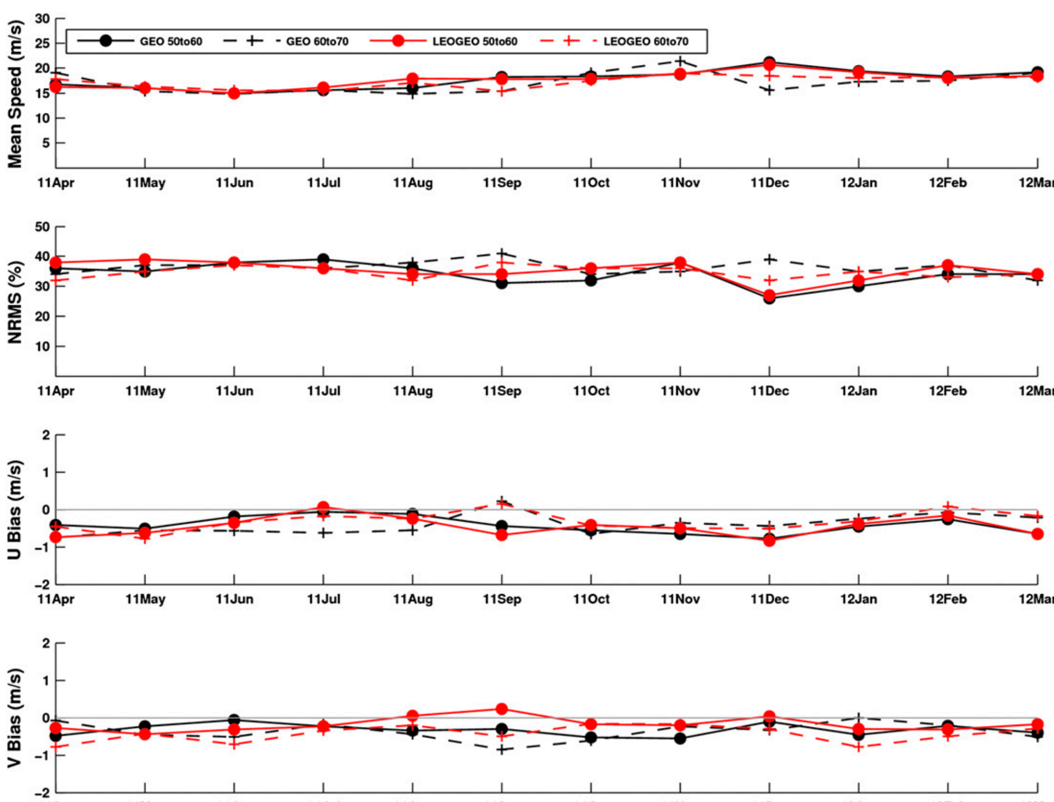

FIG. 4. April 2011–March 2012 monthly statistics of LEO–GEO mixed winds (red) and GOES-only (black) winds at two latitude bands: 50°–60°N (solid) and 60°–70°N (dashed).

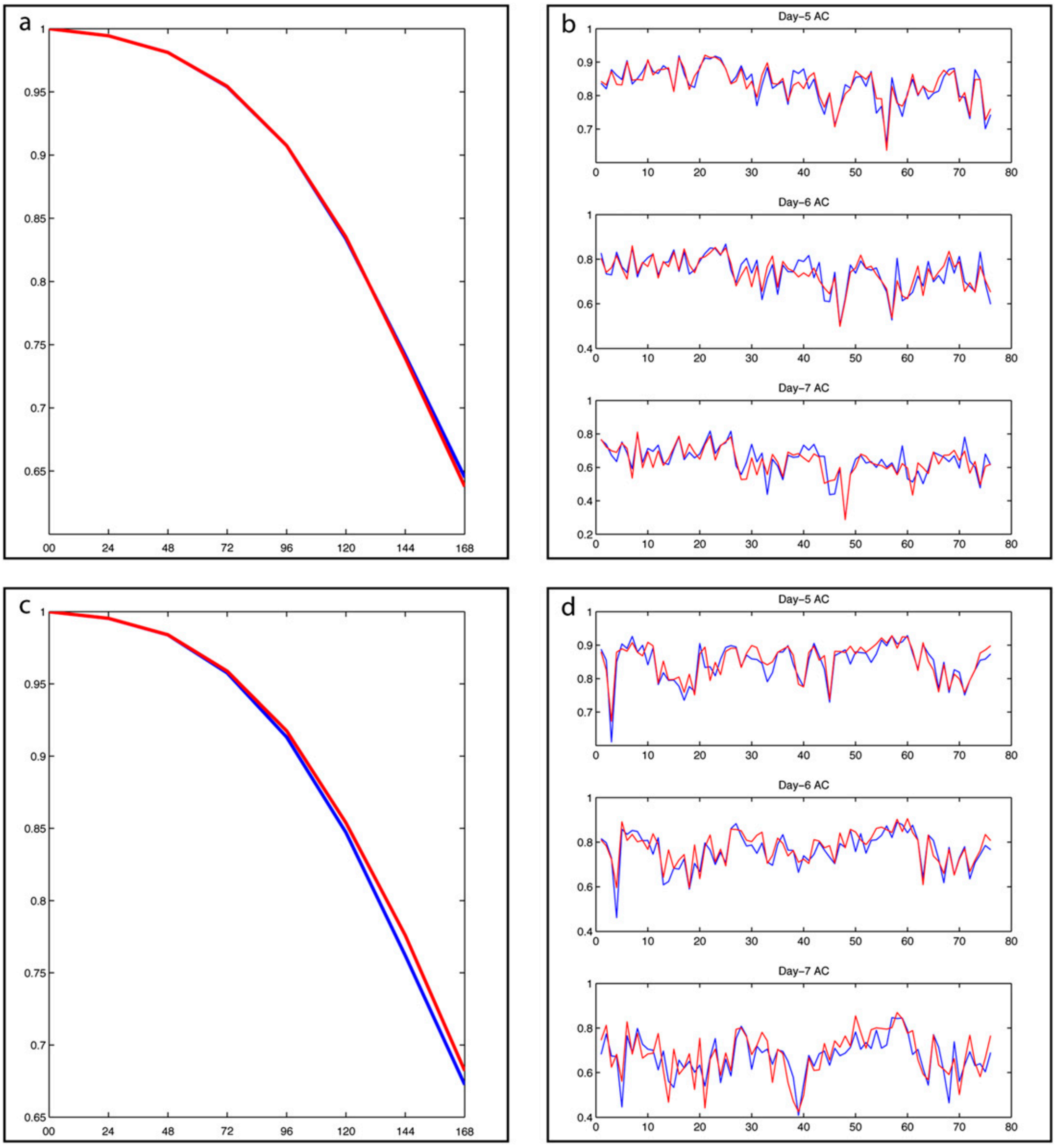

FIG. 5. Mean 500-hPa height anomaly correlations for the Southern Hemisphere cold-season experiment. The blue (red) contour represents the control (experiment) height anomaly correlation for (a) the Northern Hemisphere day-0–7 forecast; (b) the Northern Hemisphere running means for day-5, day-6, and day-7 forecasts; (c) the Southern Hemisphere day-0–7 forecast; and (d) the Southern Hemisphere running means for day-5, day-6, and day-7 forecasts.

satellite pixels; however, the parallax information is used when computing the speed and direction of the AMV.

The final blended composite images are created by retaining the pixel with the lowest area size that falls within a specified time window from the nominal image time. This results in composites containing pixels from many different satellites, varying times, and different viewing angles, with the best spatial resolution. While the composites are composed of data from a variety of satellites, each of those satellites will cover a relatively large portion or portions of the composite image.

The satellite image composites are created every 15 min using data ±15 min from a nominal image time for the infrared window channel at 4-km resolution in polar stereographic projection over each pole. The AMVs are generated using a triplet of images separated by 45 min in time. In the 50°–70° latitude bands, about 65% of the winds are from GEO-only data, 25% are from a mix of LEO/GEO satellites, and 10% are from LEO-only satellites. The composites are generated 3 h delayed from real time, the AMVs are labeled with the middle image time (45 min earlier), and the processing takes

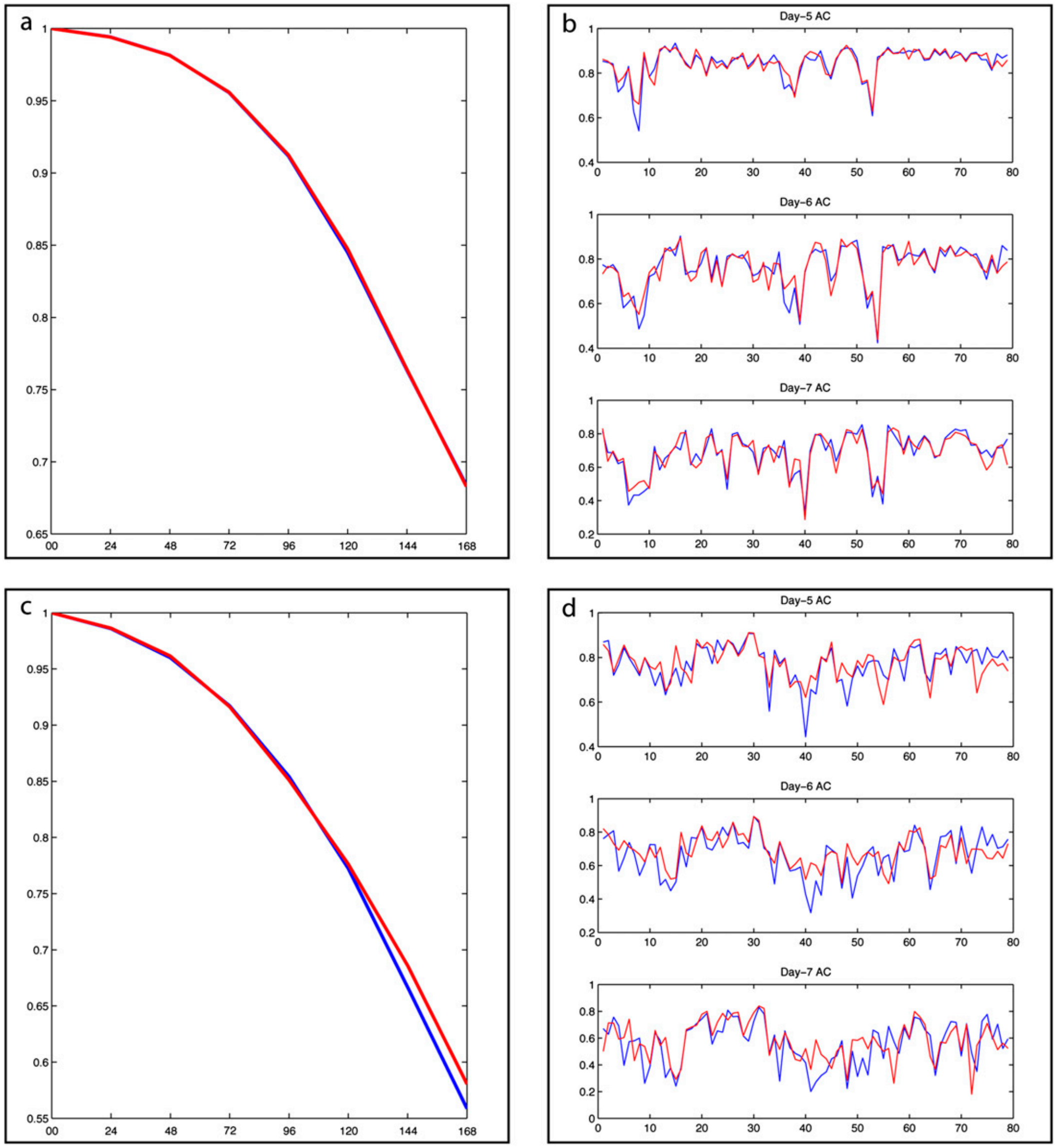

FIG. 6. As in Fig. 5, but for the Northern Hemisphere cold-season experiment.

about 5 min for each pole. Therefore, the actual delay from the observation time is approximately 3 h 50 min.

3. Validation of composite LEO–GEO AMVs

To assess the quality of the LEO–GEO AMVs, a significant sample was collected from the period 2011 into 2012 and compared with collocated rawinsondes. Because of the paucity of rawinsondes over the Southern Hemisphere, the majority of collocation matches occur over the Northern Hemisphere. A 100-km horizontal distance criterion is used, with nominal rawinsonde and AMV observation times the same (either 0000 or 1200 UTC) and to the closest rawinsonde pressure level interpolated in 10-mb increments from the original sounding that includes all mandatory and significant levels. The actual observation time of the middle satellite image (rawinsonde) could be within 15 (60) min of nominal time; therefore, it would be expected that the difference in time should be within 75 min. The validation results are partitioned by hemisphere, tropospheric layers (Table 2), and latitude bands (Table 3). The latitude band between 60° and 70° is the primary region of interest because of the aforementioned gap in regular AMV coverage.

The results in Table 2 indicate a vector root-mean-square error (RMSE) of 6.3 m s^{-1} in the Northern Hemisphere and 8 m s^{-1} in the Southern Hemisphere, where

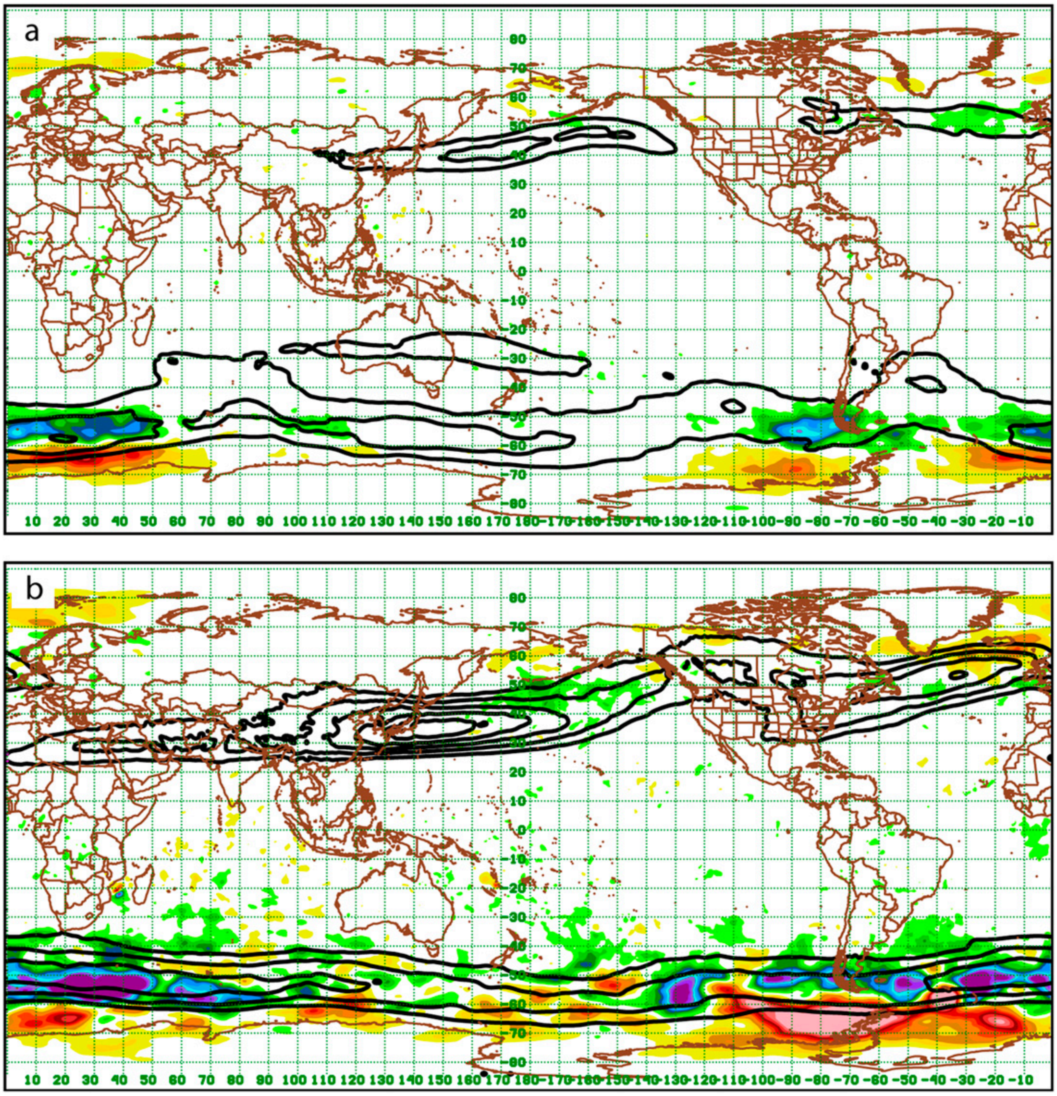

FIG. 7. Mean 300-hPa geopotential height gradient from the control simulation (black contours every $5 \times 10^{-5}\,s^{-1}$ above $20 \times 10^{-5}\,s^{-1}$), and differences in 300-hPa geopotential height between the LEO–GEO experiment and the control experiment (shaded every 0.5 m; green, blue, and purple colors are negative) for the (a) Southern Hemisphere and (b) Northern Hemisphere cold seasons.

$$\mathrm{RMSE} = \left[\frac{\sum(s_{\mathrm{sat}} - s_{\mathrm{raob}})^2}{n}\right]^{1/2}.$$

This is similar to the 6–7 m s^{-1} values for GOES-derived winds (Nieman et al. 1997; Velden et al. 1997, 2005), and 8 m s^{-1} values for LEO-derived winds (Santek 2010; Dworak and Key 2009). Over the Northern Hemisphere, the LEO–GEO AMVs generally have a small slow speed bias, which is consistent with other satellite-derived AMVs (Santek 2010; Velden et al. 1997). For the Southern Hemisphere, the overall sample speed bias tends to be smaller resulting from a fast bias in lower-level vectors. However, the collocation match counts are much smaller, making the validation results over the Southern Hemisphere less significant. When the RMSE values are normalized by the average AMV wind speed in each tropospheric layer, the results show that the smallest normalized RMSE (NRMS) value is found in the highest layer (Table 2). This is an indication that by this metric, the relative difference of the LEO–GEO AMVs compared to rawinsondes decreases with height. A similar finding has been observed for AVHRR AMVs (Dworak and Key 2009). The NRMS decrease with height is likely the product of QI. The purpose of the QI is to throw out poor quality (<0.6) winds, and has been

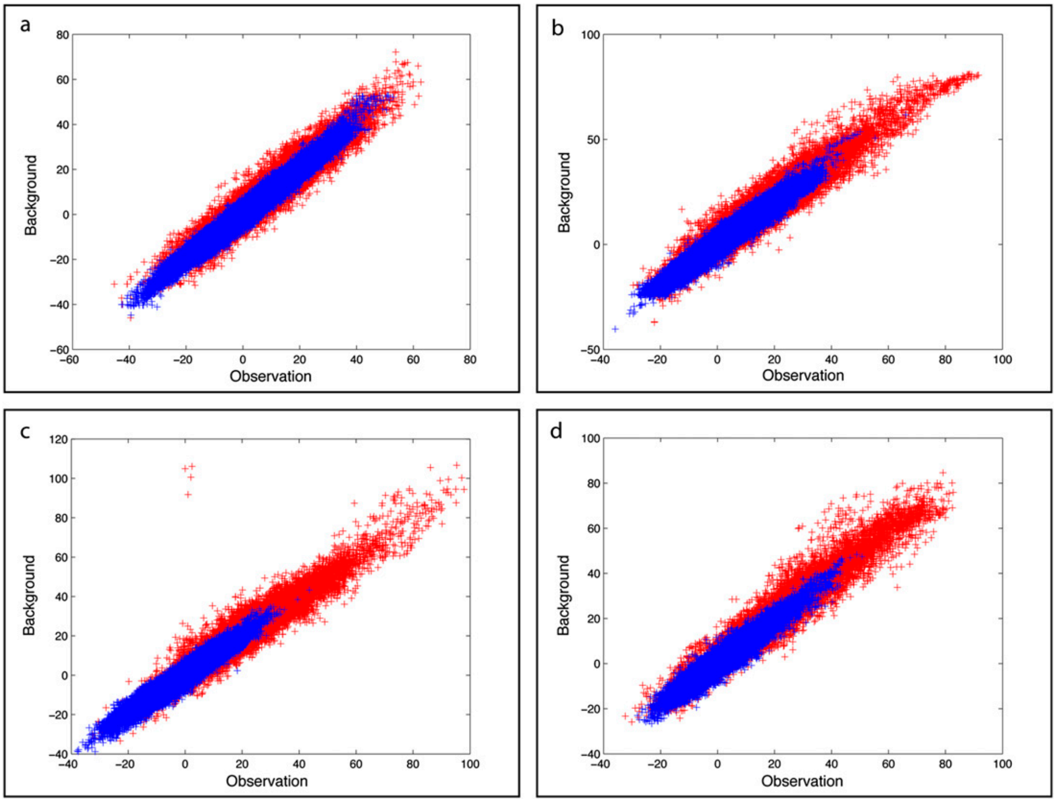

FIG. 8. Comparison of observed vs background zonal wind values for conventional MODIS AMVs (blue) and LEO–GEO AMVs (red) observed in the (a) Northern and (b) Southern Hemispheres during the Southern Hemisphere cold season, and in the (c) Northern and (d) Southern Hemispheres during the Northern Hemisphere cold season. Each set of observations is defined by a set of 5000 random observations collected at every 0000 UTC time for the periods (a),(b) 1–10 Jun 2011 and (c),(d) 1–10 Jan 2012. The background is defined as the 6-h forecast state initiated from the previous analysis, interpolated to the observation location.

shown to do a good job for high-level IR winds; however, the ability to do so for low- and midlevel winds has been shown to be poor (Holmlund 1998).

The validation results are broken down into latitude bands: 50°–60°, 60°–70°, and above 70° (Table 3). The highest quality AMVs in the Southern Hemisphere are observed to occur in the 50°–60° latitude band while in the Northern Hemisphere both the 50°–60° and 60°–70° bands have similar NRMS values. For the GEO component of the composite AMVs, Table 4 shows the highest quality winds in the Northern Hemisphere are in the 50°–60°N band; however, over the Southern Hemisphere a higher RMSE is observed over the 50°–60° band, perhaps as a result of more frequent jet streak activity during the validation period. Overall in the 60°–70° latitude bands of most interest to this study, the LEO–GEO AMVs have lower NRMS values than does GEO alone. Compared to the other two components, the LEO-only component is shown in Table 5 to have the lower RMSE, but with much smaller sample sizes equatorward of 70° because of the limited area of consecutive overlaps. Most interestingly, LEO winds over the Northern Hemisphere are shown to have improved NRMSs for the lower-latitude bands. This shows the ability of the QI to retain good quality LEO winds even at lower latitudes and that greater average AMV wind speeds are generally associated with lower NRMSs. This is likely a product of the QI, which retains more winds in faster flow regimes (Holmlund et al. 2001) that are more common in jet streaks, which are more likely to occur equatorward of 70°.

With both GEO and LEO–GEO AMV NRMS statistics being relatively similar over the validation period (Fig. 4), there is impetus to study whether the LEO–GEO AMVs can have positive NWP impacts not only on analyses over the 60°–70° latitude band, but also equatorward of 60°, and whether GEO AMVs can also have a positive impact on analyses poleward of 60°. The maximum average wind speed occurs in November (December) in the 60°–70°N (50°–60°N) latitude band. The mix of LEO–GEO AMVs for the majority of the year have a lower NRMS difference than GEO in the 60°–70°N latitude band. This is especially evident in August,

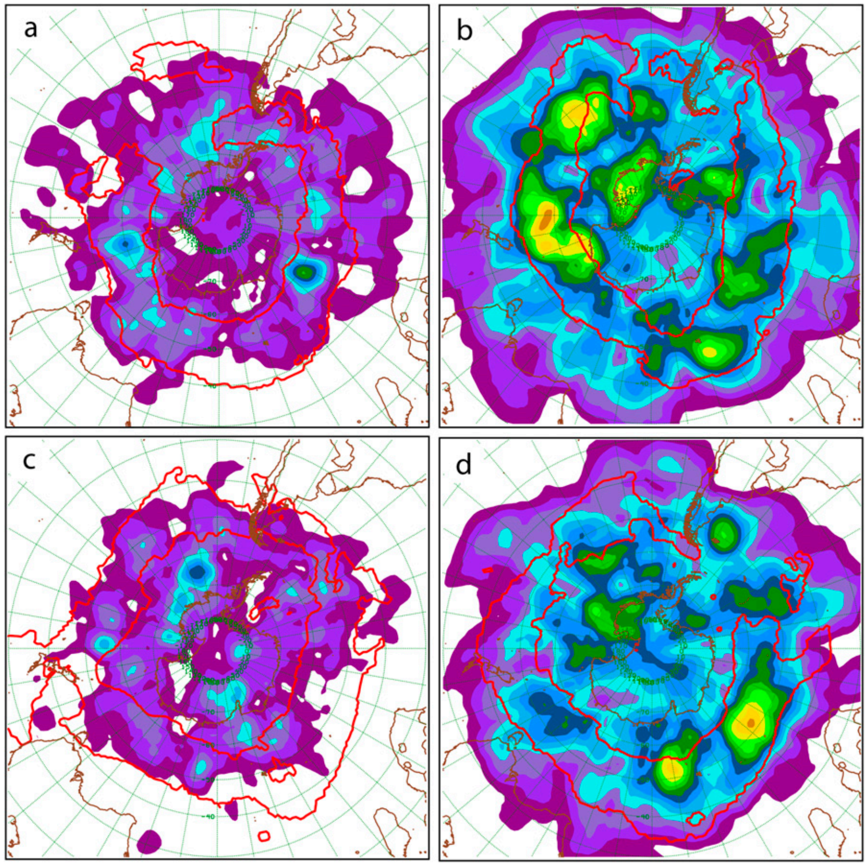

FIG. 9. Mean errors in the 500-hPa geopotential heights for the most improved forecasts at (a) 96 and (b) 168 h and for the most degraded forecasts at (c) 96 and (b) 168 h, calculated as the root of the squared difference between the control forecast and a verifying analysis (shaded every 12 m above 36 m). The location of the midlatitude jets in the mean verifying analysis is provided by the red contour, representing a 2×10^{-4} height gradient.

September, December, and February. There is even slight improvement in the NRMS for LEO–GEO over GEO in the 50°–60°N band during the summer (July–August). Biases are similar with a near-neutral to negative bias (from 0 to $-1\ \mathrm{m\,s^{-1}}$) being prevalent for most of the year period. Slow speed bias has been observed in other AMV wind products as well; however, a new nesting tracking method is showing the potential to correct for the bias (Bresky et al. 2012). GEO AMVs are traditionally not processed operationally poleward of 60°–65° latitude because of concerns regarding parallax and height assignment issues.

4. Forecast impact

Two experiments are carried out assimilating LEO–GEO AMVs into NCEP's Global Data Assimilation System (GDAS) for the GFS to assess the impact on numerical forecasts out to 7 days. Each experiment covers a period representing a cold season for each hemisphere: a 12-week experiment from 2 May to 24 July 2011, and an 11-week experiment from 23 November 2011 to 9 February 2012. The GDAS assimilates the AMVs every 6 h, and the GFS produces a 168-h forecast from 0000 UTC for every corresponding analysis during the periods of interest. The LEO–GEO AMVs are assimilated at the same time as conventional AMVs, and are constrained by excluding any vector with a QI value below 0.75, but otherwise are treated by the GDAS quality control algorithm in the same way as operational AMVs.

Forecast impact is typically evaluated in terms of the anomaly correlation, which in this case is the correlation between the forecast geopotential height anomalies, with and without the AMVs, and their own analyses. The mean 500-hPa height anomaly correlation for the 7-day forecasts reveals that the majority of the LEO–GEO AMV positive forecast impact is in the Southern Hemisphere for both the Southern Hemisphere cold-season

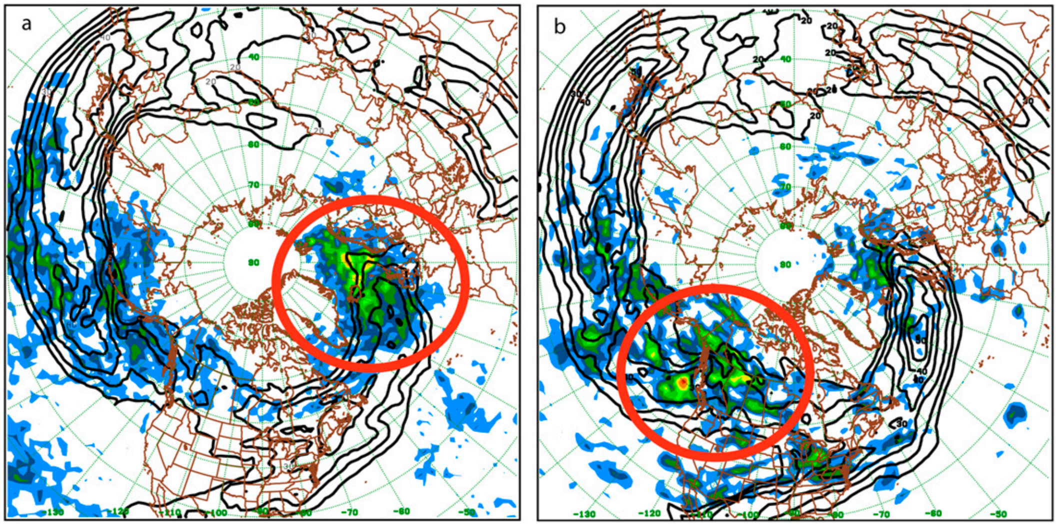

FIG. 10. (a) Difference in zonal flow at 400 hPa between the LEO–GEO experiment and analyses (control) at (a) model initialization and (b) 48 h into the forecast for the composited set of most improved forecasts. Differences are defined as the root of the squared difference relative to the control run verifying analysis, shaded every 0.5 m s^{-1} above 1 m s^{-1} at model initialization, and every 1 m s^{-1} above 5 m s^{-1} at 48 h into the forecast.

(Fig. 5) and the Northern Hemisphere cold-season (Fig. 6) experiments. This is not an unexpected result, considering that satellite data typically have a larger impact on the Southern Hemisphere analyses and forecasts (Zapotocny et al. 2007). Running day-5, day-6, and day-7 scores shows that the improvement is often constrained to forecast ''dropouts,'' which are low forecast skill events of short duration. The relative lack of dropout events in the Northern Hemisphere results in a near-neutral mean impact in both experiments, while the numerous dropout events in the Southern Hemisphere accommodate a small positive impact in both experiments, with this impact appearing at 4–5 days.

The mean analysis impact on heights near jet level is typified by a relaxation of the meridional height gradient consistent with a slowing of the winds in the 60°–70° latitude band where LEO–GEO AMVs mainly reside (Fig. 7). The analysis impact is concentrated in specific longitude bands largely consistent with each other across hemispheres, and the amplitude of the impact appears to be roughly the same in the Northern Hemisphere during both experiments. The impact in the Southern Hemisphere is stronger during the Northern Hemisphere cold season. An analysis of the observation and background statistics indicates that LEO–GEO AMVs can often sample regions of large zonal wind values in the analyses that are not sampled by conventional AMVs; this appears to be the case in the Southern Hemisphere for both seasons, but only for the Northern Hemisphere cold season (Fig. 8).

The daily score trends in Fig. 7 indicate that the LEO–GEO AMV impacts that produce the most positive results tap into specific model analysis deficiencies that result in large forecast errors; the LEO–GEO AMVs are able to reduce analysis errors in key regions and mitigate some of the error growth that results in the dropout cases. To investigate this further, composites of the 7-day forecasts for the ''most improved'' verifying analysis days are computed for cases where the mean 500-hPa height anomaly correlation for days 5–7 is improved by at least a standard deviation above the average correlation. Likewise, the ''most degraded'' forecasts are those with mean 500-hPa height anomaly correlation scores at least a standard deviation below the average.

Improvements in the Southern Hemisphere during its cold season appear to be dependent on the location of the jets with respect to where significant analysis errors appear (Fig. 9). Errors in the 500-hPa height field in the most improved 7-day forecasts mostly originate in the 60°–70° latitude band where the control forecast assimilates few AMVs. The jet structure at 500 hPa is typified by weak wave activity at low wavenumbers, allowing the jets to migrate poleward to these latitudes typically void of observations that can lead to cases of rapid analysis error growth. In contrast, the cases that profited the least from assimilating LEO–GEO AMVs appear to occur when low-wavenumber wave activity is strong, pushing the jets equatorward of this latitude band and diminishing the likelihood of the LEO–GEO AMVs to reduce analysis errors and improve 7-day forecasts.

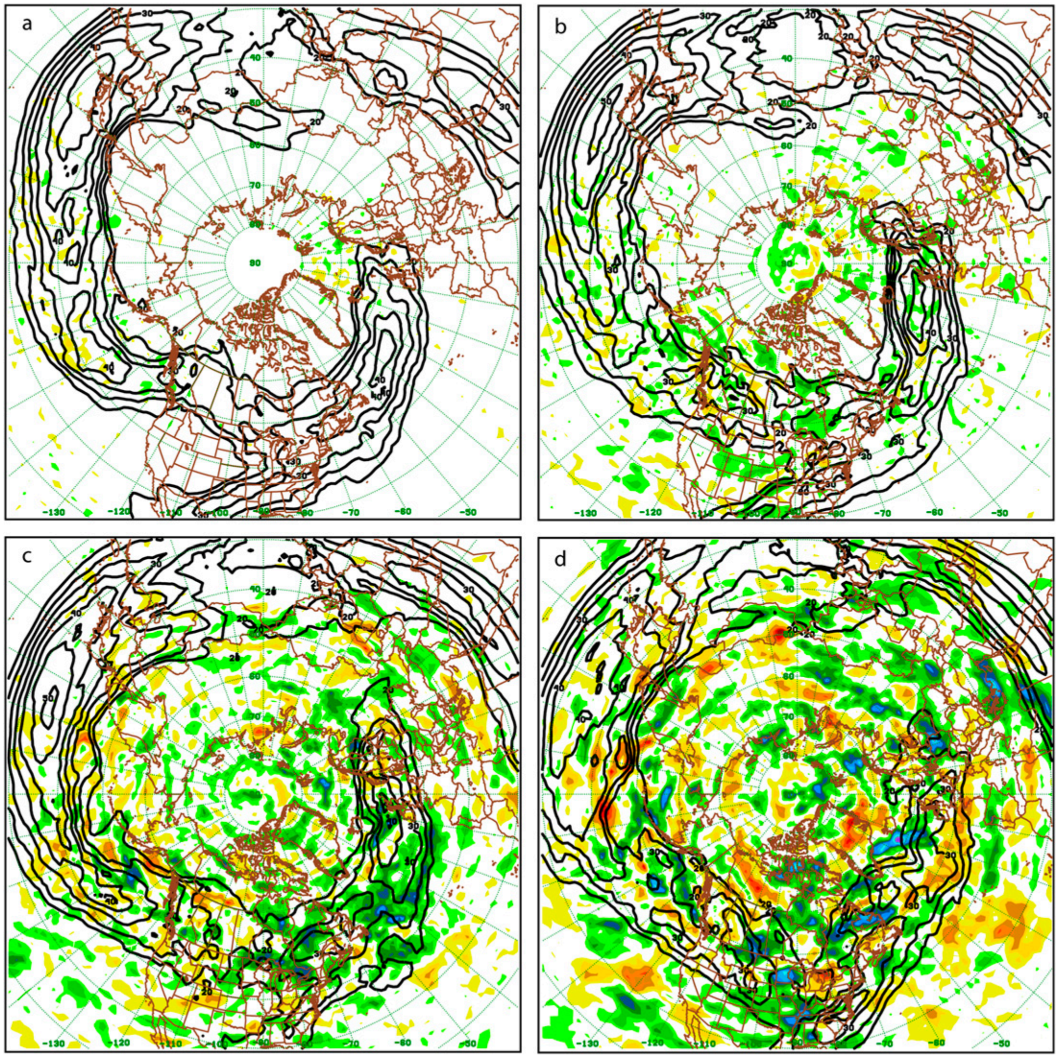

FIG. 11. Composite errors difference (experiment minus control) in 400-hPa zonal wind (shaded) for the most improved forecasts at (a) 24, (b) 72, (c) 120, and (d) 168 h. Errors are calculated as the root of the squared difference between the control forecast and the control run's verifying analysis (shaded every 1 m s^{-1}, with green and blue colors negative), with the 400-hPa composite wind speed (contoured every 5 m s^{-1} above 20 m s^{-1}) from verifying analyses overlaid.

In the Northern Hemisphere during its cold season, much of the analysis increment from LEO–GEO AMVs in zonal flow near jet level (400 hPa) appears in a diffluent region between Greenland and the coast of western Europe (Fig. 10). While this is a site of relatively larger analysis increments than those found over the North Pacific, the errors in the mean 48-h forecast for the most improved cases actually come from the Pacific jet on the west coast of North America. It is these errors over the Pacific, crossing the mainland United States and entering the Atlantic through a confluence of the polar and subtropical jets, that are reduced the most by the AMVs (Fig. 11). The origin and growth of errors is the same for the most degraded cases, though the jets themselves evolve differently, with a retraction of the Pacific jet and an intensification of the Atlantic polar/subtropical jet (not shown).

5. Conclusions

It is shown that quality AMVs can be successfully generated from high-latitude composite satellite images produced from blended geostationary and polar-orbiting platforms. Validation statistics against available collocated rawinsonde observations indicate that normalized root-mean-square errors for the composite LEO–GEO AMV have a small 1% improvement in the Northern Hemisphere and modest 6% improvement in the Southern

Hemisphere over GEO AMVs in the normally data-void 60°–70° latitude band. This study suggests that not only does the composite imagery have qualitative value for high-latitude forecasters, but it also has the potential to derive AMVs for numerical weather prediction. A two-season impact study of these AMVs in the GFS model shows a near-neutral mean impact in the Northern Hemisphere, and a small but consistent positive impact in the Southern Hemisphere with a tendency to improve the larger-magnitude low-skill forecast ''drop-out'' events. Forecasts in the Southern Hemisphere tend to be most improved in the Northern Hemisphere cold season when the jet migrates to higher latitudes and would otherwise cause rapidly growing analysis errors in the 60°–70° latitude band. In the Northern Hemisphere, LEO–GEO AMVs tend to mitigate analysis errors appearing along the nose of the eastern Pacific jet, which grow as they cross the mainland United States and interact with the Atlantic polar and subtropical jets.

The LEO–GEO winds product is being used routinely in the Naval Research Laboratory Atmospheric Variational Data Assimilation System Accelerated Representer (NAVDAS-AR) since November 2010 and at the National Center for Atmospheric Research in their Antarctic Mesoscale Prediction System (AMPS) model beginning in August 2011 (Hoover et al. 2012). The AMVs are used experimentally in the National Aeronautics and Space Administration Global Modeling and Assimilation Office (GMAO) Goddard Earth Observing System Model, version 5 (GEOS-5), and are being monitored by the Met Office. (Readers are encouraged to contact the lead author for near-real-time access to the LEO–GEO winds via ftp.) Future work aims to tune the QC for these winds, as numerical models have assimilated few if any winds in this latitudinal belt. Additional study would include a longer test to evaluate the statistical significance of the inclusion of the LEO–GEO AMVs in the numerical model.

Acknowledgments. The authors thank Rick Kohrs, Jerrold Robaidek, and Nick Bearson at SSEC for their assistance with the timely retrieval of the input satellite data used in building the composites. Thanks are given to three anonymous reviewers for their helpful input in improving this manuscript. This material is based upon work supported by the Office of Polar Programs at the National Science Foundation (ANT-0537827, ANT-0838834, ANT-1141908, and ARC-0713843, and NOAA grant NA10NES4400013). The views, opinions, and findings contained in this report are those of the authors and should not be construed as an official National Oceanic and Atmospheric Administration or U.S. government position, policy, or decision.

REFERENCES

Bresky, W. C., J. M. Daniels, A. A. Bailey, and S. T. Wanzong, 2012: New methods towards minimizing the slow speed bias associated with atmospheric motion vectors. *J. Applied Meteor. Climatol.,* **51,** 2137–2151.

Dworak, R., and J. R., Key, 2009: Twenty years of polar winds from AVHRR: Validation and comparison with ERA-40. *J. Applied Meteor. Climatol.,* **48,** 24–40.

Holmlund, K., 1998: The utilization of statistical properties of satellite-derived atmospheric motion vectors to derive quality indicators. *Wea. Forecasting,* **13,** 1093–1104.

——, C. S. Velden, and M. Rohn, 2001: Enhanced automated quality control applied to high-density satellite winds. *Mon. Wea. Rev.,* **129,** 517–529.

Hoover, B., D. Santek, M. Lazzara, R. Dworak, J. Key, C. Velden, and N. Bearson, 2012. High latitude satellite-derived winds from combined geostationary and polar orbiting satellite data. *Proc. 11th Int. Winds Workshop,* Auckland, New Zealand, EUMETSAT. [Available online at http://cimss.ssec.wisc.edu/iwwg/iww11/iww11_programme.html.]

Joyce, R., J. Janowiak, and G. Huffman, 2001: Latitudinally and seasonally dependent zenith-angle corrections for geostationary satellite IR brightness temperatures. *J. Appl. Meteor.,* **40,** 689–703.

Key, J. R., D. A. Santek, C. S. Velden, N. Bormann, J.-N. Thepaut, L. P. Riishojgaard, Y. Zhu, and W. P. Menzel, 2003: Cloud-drift and water vapor winds in the polar regions from MODIS. *IEEE Trans. Geosci. Remote Sens.,* **41,** 482–492.

Kohrs, R. A., M. A. Lazzara, J. O. Robaidek, D. A. Santek, and S. L. Knuth, 2013: Global satellite composites—20 years of evolution. *Atmos. Res.,* **135–136,** 8–34, doi:10.1016/j.atmosres.2013.07.023.

Lazzara, M. A., and S. L. Knuth, 2009: Arctic satellite composites observations: A new perspective. *Proc. 10th Conf. on Polar Meteorology and Oceanography,* Madison, WI, Amer. Meteor. Soc., 13.1. [Available online at https://ams.confex.com/ams/pdfpapers/152725.pdf.]

——, C. R. Stearns, J. A. Staude, and S. L. Knuth, 2003: 10 years of Antarctic composite images. Preprints, *Seventh Conf. on Polar Meteorology and Oceanography/Joint Symp. on High-Latitude Climate Variations,* Hyannis, MA, Amer. Meteor. Soc., 9.4. [Available online at https://ams.confex.com/ams/pdfpapers/60787.pdf.]

——, R. Dworak, D. A. Santek, C. S. Velden, and J. R. Key, 2010: High latitude atmospheric motion vectors: Application of Antarctic and Arctic composite satellite imagery. *Proc. 10th Intl. Winds Workshop,* Tokyo, Japan, EUMETSAT, 6 pp. [Available online at http://www.eumetsat.int/Home/Main/AboutEU-METSAT/Publications/ConferenceandWorkshopProceedings/2010/groups/cps/documents/document/pdf_conf_p56_s5_05_dworak_v.pdf.]

——, A. Coletti, and B. L. Diedrich, 2011: The possibilities of polar meteorology, environmental remote sensing, communications and space weather applications from Artificial Lagrange Orbit Polar Satellite Composite Imagery. *Adv. Space Res.,* **48,** 1880–1889, doi:10.1016/j.asr.2011.04.026.

Minnis, P., 1989: Viewing zenith-angle dependence of cloudiness determined from coincident GOES East and GOES West data. *J. Geol. Res.,* **94,** 2303–2320.

Nieman, S. J., W. P. Menzel, C. M. Hayden, D. Gray, S. T. Wanzong, C. S. Velden, and J. Daniels, 1997: Fully automated cloud-drift winds in NESDIS operations. *Bull. Amer. Meteor. Soc.,* **78,** 1121–1133.

Palmén, E., and C. Newton, 1969: *Atmospheric Circulation Systems: Their Structure and Physical Interpretation.* Academic Press, 603 pp.

Santek, D. A., 2010: The impact of satellite-derived polar winds on lower-latitude forecasts. *Mon. Wea. Rev.,* **138,** 123–139.

Velden, C. S., C. M. Hayden, S. J. Nieman, W. P. Menzel, S. Wanzong, and J. S. Goerss, 1997: Upper-tropospheric winds derived from geostationary satellite water vapor observations. *Bull. Amer. Meteor. Soc.,* **78,** 173–195.

——, and Coauthors, 2005: Recent innovations in deriving tropospheric winds from meteorological satellites. *Bull. Amer. Meteor. Soc.,* **86,** 205–223.

Zapotocny, T. H., J. A. Jung, J. F. Le Marshall, and R. F. Treadon, 2007: A two-season impact study of satellite and in situ data in the NCEP Global Data Assimilation System. *Wea. Forecasting,* **22,** 887–909.